Supplementary material

Water Research **2021**, article no. 117300.
DOI: https://doi.org/10.1016/j.watres.2021.117300

Carbon and methane cycling in arsenic-contaminated aquifers

Emiliano Stopelli[1,11,*], Vu T. Duyen[2], Henning Prommer[3,4], Martyna Glodowska[5], Andreas Kappler[5], Magnus Schneider[6], Elisabeth Eiche[6], Alexandra K. Lightfoot[1], AdvectAs team members[7], Carsten J. Schubert[8,9], Pham K.T. Trang[2], Pham H. Viet[2], Rolf Kipfer[1,9], Lenny H.E. Winkel[1,9], and Michael Berg[1,10,*]

[1]Eawag, Swiss Federal Institute of Aquatic Science and Technology, Department Water Resources and Drinking Water, 8600 Dübendorf, Switzerland. [2]Key Laboratory of Analytical Technology for Environmental Quality and Food Safety (KLATEFOS), VNU University of Science, Vietnam National University, Hanoi, Vietnam. [3]CSIRO Land and Water, 6014 Floreat, Western Australia, Australia. [4]School of Earth Sciences, University of Western Australia, Crawley, WA 6009, Australia. [5]Geomicrobiology, Center for Applied Geosciences, University of Tübingen, 72076 Tübingen, Germany. [6]Institute of Applied Geosciences, Karlsruhe Institute of Technology, 76131 Karlsruhe, Germany. [7]AdvectAs team members (see below). [8]Eawag, Swiss Federal Institute of Aquatic Science and Technology, Department Surface Waters Research & Management, 6047 Kastanienbaum, Switzerland. [9]Institute of Biogeochemistry and Pollutant Dynamics, ETH Zurich, 8092 Zurich, Switzerland. [10]UNESCO Chair on Groundwater Arsenic within the 2030 Agenda for Sustainable Development, School of Civil Engineering and Surveying, University of Southern Queensland, QLD 4350, Australia. [11]Present address: Nagra, National Cooperative for the Disposal of Radioactive Waste, International Services and Projects, 5430 Wettingen, Switzerland.

** Corresponding authors: Emiliano Stopelli (emiliano.stopelli@eawag.ch), Michael Berg (michael.berg@eawag.ch)*

Highlights

- Comprehensive carbon isotope analyses for δ13C-DOC, δ13C-DIC and δ13C-CH4 provide novel insights
- Occurrence of fermentation, methanogenesis and methanotrophy was identified
- Locally depositional organic matter promotes methanogenesis and very high As concentrations
- Methane cycling could play an overlooked role in many high-As aquifers around the world
- Identified processes are triggers for the elusive heterogeneity of As concentrations in groundwater

Graphical abstract

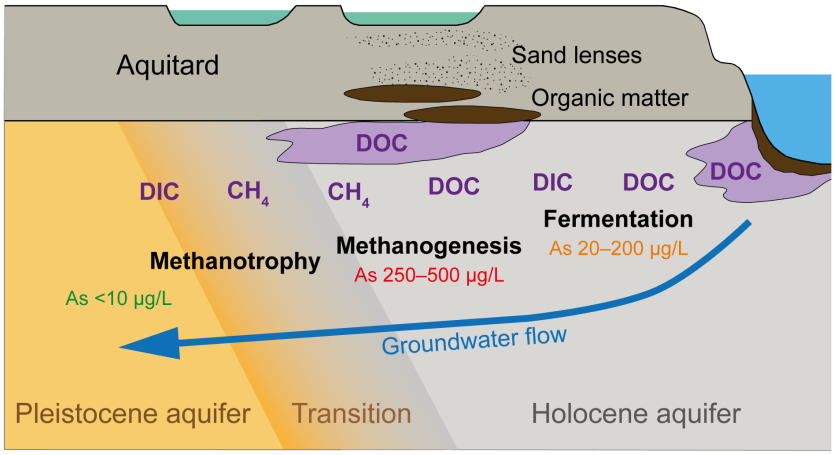

Supplementary material

Contents

AdvectAs team members

Karlsruhe Institute of Technology - Institute of Applied Geosciences: M. Schneider, Dr. E. Eiche, Prof. Dr. A. Kontny

Technical University of Berlin - Institute of Applied Geosciences: Prof. Dr. T. Neumann

University of Tübingen - Department of Geosciences: Dr. M. Glodowska, Dr. B. Rathi, Prof. Dr. A. Kappler, Jun.-Prof. Dr. S. Kleindienst, Prof. Dr.-Ing. O. A. Cirpka

Eawag, Swiss Federal Institute of Aquatic Science and Technology - Department of Water Resources and Drinking Water: A. Lightfoot, Dr. E. Stopelli, Prof. Dr. M. Berg, Prof. Dr. R. Kipfer, Prof. Dr. L. Winkel

Vietnam National University, Hanoi - Key Laboratory of Analytical Technology for Environmental Quality and Food Safety Control (KLATEFOS): Vu T. Duyen, Tran T. Mai, Vi M. Lan, Dao V. Nga, Dr. Pham T.K. Trang, Prof. Dr. Pham H. Viet

The University of Western Australia and CSIRO Land and Water: Prof. Dr. Henning Prommer

Table S1: Hydrochemical parameters measured in surface waters and groundwater t Van Phuc near Hanoi (Vietnam)

					method	sensor	sensor	sensor	sensor	sensor	ICP-MS	ICP-MS	ICP-MS	ICP-MS	ICP-MS	ICP-MS	ICP-MS	ICP-MS
					LOQ						0.1	0.02	0.002	0.05	0.1	0.2	0.1	0.01
					unit	°C		mg/L	µS/cm	mV (SHE)	µgAs/L	mgFe/L	mgMn/L	mgS/L	mgNa/L	mgK/L	mgCa/L	mgMg/L
Place ID	**Simplified ID**	**Distance from river km**	**Depth (m bgl)**	**latitude N**	**longitude E**	**t**	**pH**	**O_2**	**conductivity**	**E_h**	**As**	**Fe**	**Mn**	**S**	**Na**	**K**	**Ca**	**Mg**
Red River 1	**R1**	0	0.00	20°55'38.1''	105°53'50.8''	24.3	9.53	7.59	212	332	1.6	<0.02	0.002	2.6	3.3	1.6	26	5.0
Red River 2	**R2**	0	0.00	20°54'46.0''	105°54'25.1''	25.5	9.53	7.78	227	323	1.4	<0.02	0.004	2.7	3.1	1.5	27	4.9
Red River 3	**R3**	0	0.00	20°54'24.4''	105°53'52.1''	24.8	8.94	7.53	237	418	2.0	<0.02	0.018	2.8	4.1	2.1	26	5.4
River Bank 1	**R1**	0	0.25	20°55'36.1''	105°53'56.0''	-	-	5.14	227	-	51	<0.02	0.069	2.9	3.7	1.9	27	5.5
River Bank 2	**R2**	0	0.25	20°54'46.0''	105°54'25.1''	26.5	8.87	0.63	245	324	22	<0.02	0.814	2.2	3.7	1.9	29	4.2
River Bank 3	**R3**	0	0.25	20°54'24.4''	105°53'52.1''	24.1	7.80	3.88	1270	339	23	0.02	0.943	4.1	9.2	9.4	60	16
Pond 1	**P1**	1.70	0.00	20°55'18.3''	105°53'36.7''	29.5	7.84	4.32	403	162	4.6	<0.02	0.088	5.5	11	13	40	11
Pond 2	**P2**	0.80	0.00	20°55'02.1''	105°54'01.5''	30.4	7.58	1.72	542	183	6.7	0.67	0.414	1.1	25	16	35	9.0
Pond 3	**P3**	1.80	0.00	20°55'25.8''	105°53'36.4''	25.3	8.96	4.63	511	359	8.3	<0.02	0.075	4.7	20	18	38	15
AMS15 (°)	**1**	0.10	23-24	20°55'36.4''	105°53'51.5''	25.8	8.40	0.29	661	345*	22	0.53	1.52	0.1	19	6.5	27	26
AMS12	**2**	0.21	23-24	20°54'50.9''	105°54'21.0''	27.5	7.74	0.28	930	95*	138	12	0.689	9.2	5.4	2.7	123	28
VP56	**3a**	0.54	18-19	20°54'57.9''	105° 54' 11.9''	23.2	6.65	0.52*	1386	163	100	17	0.329	0.1	38	2.3	168	36
VP57	**3b**	0.54	28-29	20°54'57.9''	105° 54' 11.9''	21.5	7.45	0.39	1037	170	203	22	0.217	<0.05	14	3.0	122	29
VP58	**3c**	0.54	38-39	20°54'57.9''	105° 54' 11.9''	24.9	7.46	0.48	1205	183	205	24	0.280	<0.05	22	3.3	142	34
AMS13 (°)	**4**	0.66	23-24	20°54'39.4''	105°53'36.7''	25.4	7.82	0.93*	1002	101*	349	7.6	0.184	0.1	13	6.3	68	30
Household well	**5**	0.85	43.5-47.5	20°55'08.3''	105°54'07.6''	26.5	7.17	0.59*	1417	150*	88	9.5	1.38	1.0	40	2.2	172	32
PC51	**6a**	1.00	18-19	20°55'04.1''	105°53'54.3''	27.7	7.26	0.21	1041	96*	385	8.7	1.00	0.1	9.0	6.9	71	29
PC52	**6b**	1.00	28-29	20°55'04.1''	105°53'54.3''	27.4	7.31	0.25	954	70	502	12	0.252	0.1	14	5.5	75	27
VP55	**6c**	1.00	38-39	20°55'04.1''	105° 53' 54.2''	26.3	7.36	0.19	1001	62	377	13	0.184	<0.05	12	5.5	89	34
VP59	**7a**	1.44	18-19	20°55'15.0''	105°53'46.2''	27.0	7.12	0.21	1058	118	394	19	0.170	<0.05	12	2.2	132	28
VPNS3	**7b**	1.44	25-26	20°55'14.9''	105°53'46.1''	26.3	7.25	0.24	1031	95*	340	19	0.165	<0.05	14	1.5	123	28
AMS5	**8a**	1.59	23-24	20°55'17.4''	105°53'41.7''	28.4	7.44	0.29	1254	95*	534	14	0.131	0.1	10	7.9	88	28
VPNS5	**8b**	1.59	35-36	20°55'17.4''	105°53'41.7''	26.1	7.36	0.28	1050	83*	352	12	0.180	<0.05	15	2.9	123	29
AMS11-25	**9a**	1.68	23-24	20°55'18.4''	105°53'38.5''	26.8	7.19	0.11	1016	57	387	11	0.502	0.0	10	5.9	97	32
AMS11-32	**9b**	1.68	30-31	20°55'18.3''	105°53'38.4''	-	7.38	0.28	994	235	2.0	0.07	1.46	<0.05	14	4.3	109	37
AMS11-47	**9c**	1.68	45-46	20°55'18.4''	105°53'38.5''	27.7	6.60	0.17	519	236	9.0	15	0.990	0.2	41	3.6	25	17
AMS31	**10a**	1.69	23-24	20°55'18.6''	105°53'38.1''	26.9	7.36	0.21	867	45	271	9.7	0.911	<0.05	9.8	4.6	87	29
PC43-28	**10b**	1.69	26-27	20°55'18.6''	105°53'38.2''	26.4	7.32	0.21	874	114*	51	8.7	2.26	<0.05	9.3	4.5	91	31
PC53	**10c**	1.69	30-31	20°55'18.8''	105°53'38.3''	26.4	7.18	0.30	975	355*	1.5	0.62	2.03	0.1	13	4.4	116	32
PC44-38	**10d**	1.69	36-37	20°55'18.5''	105°53'38.2''	26.8	7.11	0.18	939	147	2.7	0.21	2.53	0.1	18	5.2	81	55
RD54	**10e**	1.69	39.5-40.5	20°55'18.8''	105°53'38.3''	26.6	6.99	0.28	827	234	2.9	1.7	2.12	0.1	19	4.9	71	50
AMS32	**11**	1.71	23-24	20°55'18.9''	105°53'37.6''	26.4	7.83	0.25	877	87*	74	8.3	3.51	<0.05	8.3	4.6	93	24
AMS36	**12**	1.72	23-24	20°55'19.6''	105°53'37.6''	26.4	7.14	0.29	920	130	1.9	0.69	1.92	<0.05	10	3.6	120	19
AMS4	**13a**	1.75	22-23	20°55'18.9''	105°53'36.7''	26.7	7.24	0.30	862	170	1.1	0.14	1.20	<0.05	9.4	4.6	111	22
VPNS4	**13b**	1.75	36-37	20°55'18.9''	105°53'36.7''	27.0	7.09	0.29	949	271	<0.1	<0.02	1.52	<0.05	12	5.4	81	58
VPMLA-22	**14a**	1.95	20-21	20°55'23.4''	105°53'31.6''	26.5	6.93	0.35	519	196	1.0	0.09	2.33	1.6	30	3.2	31	26
VPMLA-38	**14b**	1.95	36-37	20°55'23.4''	105°53'31.6''	26.5	6.95	0.36	415	175	0.8	0.28	0.277	2.0	32	2.8	20	20
VPMLA-54	**14c**	1.95	52-53	20°55'23.4''	105°53'31.6''	26.6	7.08	0.30	603	105	7.5	23	1.12	0.4	26	4.1	29	30
Blank lab	-	-	-	-	-	-	-	-	-	-	<0.1	<0.02	<0.002	<0.05	<0.1	<0.2	<0.1	<0.01
Blank field	-	-	-	-	-	-	-	-	-	-	<0.1	<0.02	<0.002	<0.05	<0.1	<0.2	<0.1	<0.01

Table S1: continued

method		PICARRO	PICARRO	titration kit	PHREEQC	titration kit	PHREEQC	EA-IRMS	TOC	TOC	EA-IRMS	FOTOM	FOTOM	EA-IRMS	GC-TCD	GC-IRMS
LOQ***		-	-	1.2		1.2		22 mg C/L	0.5	0.5	0.5 mg C/L	0.02	0.02	0.04 mg N/L	0.13	0.1 mgCH_4/L
unit		‰ VSMOW	‰ VSMOW	mgC/L	mgC/L	mgC/L	mgC/L	‰ VPDB	mgC/L	mgC/L	‰ VPDB	mgN/L	mgN/L	‰ air	mgCH_4/L	‰ VPDB
Place ID	**Simplified ID**	**$\delta^{18}O$**	**$\delta^{2}H$**	**C-alk Apr19**	**DIC Apr19**	**C-alk Jul18**	**DIC Jul18**	**δ^{13}C-DIC**	**DOC Apr19**	**DOC Jul18**	**δ^{13}C-DOC**	**NH_4^+ Apr19**	**NH_4^+ Jul18**	**δ^{15}N-NH_4^+**	**CH_4**	**δ^{13}C-CH_4**
Red River 1	R1	-8.88	-59.66	24	18	20	23	-24.5**	0.9	1.3	-26.4	0.11	0.02	11.8**	-	-
Red River 2	R2	-8.68	-59.62	23	18	23	28	-10.5	0.9	1.2	-28.6	0.05	0.04	11.9	-	-
Red River 3	R3	-8.50	-57.91	24	22	23	28	-8.6	2.1	1.5	-28.7	0.96	0.25	6.89	-	-
River Bank 1	R1	-8.64	-58.04	26	25	35	44	-	1.4	3.3	-27.6	0.91	0.03	12.6**	-	-
River Bank 2	R2	-8.44	-56.98	-	-	40	49	-8.7	2.3	2.2	-28.0	0.61	0.02	6.45**	-	-
River Bank 3	R3	-7.41	-49.70	119	119	40	50	-9.0	12	2.4	-27.5	71	0.20	11.3	-	-
Pond 1	P1	-3.37	-30.59	42	43	35	39	-2.3	5.4	5.8	-25.2	0.47	1.8	26.1	-	-
Pond 2	P2	-3.91	-20.93	49	51	0	-	-	12	-	-	8.8	-	-	-	-
Pond 3	P3	-1.45	-16.95	47	42	48	54	-14.4	7.2	10	-	0.82	0.70	13.1	-	-
AMS15 (°)	1	-7.15	-49.13	76	71	67	89	-11.1	1.0	1.2	-30.1	24	23	3.45	<0.13	-
AMS12	2	-8.57	-58.52	77	78	113	147	-8.8 / -8.0	0.6	1.0	-30.3 / -31.3	0.64	0.66	5.23	<0.13	-10.1
VP56	3a	-8.36	-56.94	172	243	-	-	-5.2	2.5	-	-30.8	11	-	-	13	-85.4
VP57	3b	-7.33	-51.38	139	147	-	-	-5.2	2.4	-	-30.4	16	-	-	10	-
VP58	3c	-8.06	-54.14	148	155	-	-	-6.0	2.4	-	-30.9	14	-	-	6.9	-
AMS13 (°)	4	-4.49	-34.46	114	114	120	165	-1.4	6.7	7.3	-28.1	46	51	4.12	3.0	-
Household well	5	-7.63	-49.98	152	171	172	250	-3.0	1.4	1.7	-28.1	4.3	3.4	3.88	<0.13	-
PC51	6a	-5.38	-39.45	128	141	-	-	-	6.5	-	-28.8	49	-	-	40	-74.0
PC52	6b	-5.37	-39.48	116	126	-	-	0.2	5.4	-	-29.6	33	-	-	48	-
VP55	6c	-5.50	-41.46	127	137	-	-	-0.8	2.8	-	-30.7	29	-	-	21	-
VP59	7a	-6.74	-47.56	122	139	-	-	-7.4	1.8	-	-30.9	5.3	-	-	11	-86.3
VPNS3	7b	-7.19	-49.12	121	133	-	-	-	1.5	-	-	5.4	-	-	2.3	-
AMS5	8a	-6.50	-44.24	144	152	160	225	-1.8 / -0.9	7.1	8.0	-28.8 / -29.0	64	66	23.0	58	-75.4
VPNS5	8b	-7.63	-51.46	131	140	132	164	-0.8	2.2	2.3	-29.3	10	11	4.97	6.1	-86.4
AMS11-25	9a	-5.70	-40.69	122	137	120	149	2.9 / 6.2	4.0	3.3	-29.4 / -29.7	26	26	4.62	37	-78.4
AMS11-32	9b	-6.77	-47.77	115	124	118	151	-	0.8	1.2	-28.5	9.3	10	5.24	<0.13	-20.8
AMS11-47	9c	-7.41	-50.18	62	94	-	-	-9.2	0.8	1.1	-30.2	0.57	0.50	5.22	0.18	-
AMS31	10a	-5.49	-39.95	107	115	120	153	-3.5	2.8	3.5	-29.6	18	21	4.14	16	-87.1
PC43-28	10b	-5.29	-40.60	107	116	107	135	-0.6	1.8	3.7	-29.3	16	16	5.11	14	-80.6
PC53	10c	-7.07	-48.76	118	132	-	-	-8.7	0.7	-	-30.8	5.7	-	-	<0.13	-
PC44-38	10d	-7.55	-51.68	116	133	121	177	-5.8	0.6	0.9	-29.1	0.98	1.2	5.44	<0.13	-37.6
RD54	10e	-7.89	-53.73	107	128	-	-	-8.8	0.8	-	-31.2	1.6	-	-	<0.13	-
AMS32	11	-5.04	-38.34	108	108	122	151	-5.6 / -7.3	2.0	2.3	-29.7 / -30.5	16	18	5.08	19	-79.4
AMS36	12	-5.49	-39.52	108	123	104	135	-17.0	1.3	1.4	-30.7	12	13	5.29	0.38	-2.20
AMS4	13a	-5.58	-40.08	104	116	107	145	-10.5 / -9.5	0.9	1.2	-29.8 / -31.4	12	13	7.01	<0.13	46.4
VPNS4	13b	-5.65	-40.70	119	137	110	162	-5.6	0.6	0.9	-30.4	3.0	2.8	4.84	<0.13	-
VPMLA-22	14a	-6.87	-45.92	67	83	30 (24 m)	96	-12.6 / -10.1	<0.5	1.3 (24 m)	-30.6 / -31.7	0.17	0.09	6.13	<0.13	-
VPMLA-38	14b	-6.50	-44.32	52	63	55	113	-11.4	0.6	0.7	-29.6	0.11	0.12	5.79	<0.13	-
VPMLA-54	14c	-7.19	-48.56	76	87	77	131	-6.4	0.5	0.7	-30.2	0.64	0.65	4.91	<0.13	-
Blank lab	-	-	-	-	-	-	-	-	<0.5	<0.5	-	<0.02	<0.02	-	-	-
Blank field	-	-	-	-	-	-	-	-	<0.5	<0.5	-	<0.02	<0.02	-	-	-

°Wells close to the transect under study *Suspect sensor values compared to Stopelli et al., 2020. Probable oxidation within the flow cell used for sensors **Uncertain isotopic value due to low mass quantity analysed ***For stable isotopes, LOQ is also dependent on the sampled volume

SI.1 Linear mixing model calculations at the aquitard/aquifer hydraulic connections

Step 1: Determination of water sources mix from $\delta^{18}O$-H_2O and $\delta^{2}H$-H_2O, subsequent DOC mass-balance calculations

Assumptions and notes:

- Applied the linear mixing model calculations (IAEA, 2001)

$$\delta_{MIX} = f_1 \cdot \delta_{X1} + f_2 \cdot \delta_{X2}, \text{ with } f_1 + f_2 = 1$$

- $\delta^{18}O$-H_2O and $\delta^{2}H$-H_2O are conservative and related only to the source of water;
- Based on hydrochemical data, we assume two sources of water at the aquitard/aquifer connections: aquitard/pond water (X_1) and Holocene aquifer water (X_2);
- Ponds are representative of both natural and anthropogenic surficial waters undergoing evaporation;
- Values of pore water at 16-18 m correspond to aquitard/aquifer hydraulic connections and include pond water. In fact, surficial water must percolate through the aquitard to reach the aquifer. This vertical movement allows for the mixing and smoothing of the large yearly isotopic variability measured in pond samples (Stopelli et al., 2020). Pond values for $\delta^{18}O$ range from -1±0.5‰ to -9±0.5‰ and for $\delta^{2}H$ from -20±3‰ to -60±3‰. Average values coincide with the aquitard pore water value employed in the mixing model;
- Aquitard sediments were collected with piston cores at the location of multiple well 6 and frozen until the analyses. Frozen sediments were thawed for two days at +4°C, and pore water was extracted under argon (to minimise the risk of sediment and pore water oxidation) in the laboratory with a GEOTEK pore water device (http://www.geotek.co.uk). Pore water was filtered through a glass fibre pre-filter (Sartorius, Item No. 13400–100, diameter 100 mm) followed by 0.45-µm CA filters. The pore water aliquot collection, preservation and analyses followed the same procedure reported in the Methodology for the groundwater samples.

	$\delta^{18}O$ aquitard pore water at well 6, 16-18m **X_1, aquitard+pond**	$\delta^{18}O$ wells 2 and 3 **X_2, Holocene aquifer**	$\delta^{18}O$ wells 6 and 8 **Aquitard/aquifer connection**
$\delta^{18}O$ ‰	-5.8 (-5.3/-6.3)	-8.5 (-8.4/-8.6)	-6.0 (-5.4/-6.5)
Resulting mix	**0.92**	**0.08**	

	$\delta^{2}H$ aquitard pore water at well 6, 16-18m **X_1, aquitard+pond**	$\delta^{2}H$ wells 2 and 3 **X_2, Holocene aquifer**	$\delta^{2}H$ wells 6 and 8 **Aquitard/aquifer connection**
$\delta^{2}H$ ‰	-41.5 (-39/-44)	-57.5 (-57/-58)	-42.5 (-40/-45)
Resulting mix	**0.93**	**0.07**	

In the further step, we used the averaged contribution of the pond/aquitard of 92% and Holocene aquifer water of 8%.

	DOC aquitard pore water at well 6, 16-18m **X_1, aquitard+pond**	DOC wells 2 and 3 **X_2, Holocene aquifer**	DOC wells 6 and 8 **Aquitard/aquifer connection**
DOC mg C/L	5-8	0.6-2.5	**6.5-7 real**
Mixing ratio from $\delta^{18}O$/ $\delta^{2}H$	0.92	0.08	
C budget mg C/L	**4.6-7.4**	**0.05-0.2**	**4.6-7.6 model**

The mixing model based on $\delta^{18}O$ and $\delta^{2}H$ gives a realistic estimation of the range of DOC concentrations. The simulation with water isotopes provides a likely mass balance for DOC and indicates a large relative local input of water from the pond/aquitard in wells with large concentrations of DOC and methane, thereby suggesting disrupted groundwater flow conditions associated with methanogenesis.

Step 2: Mix of C sources from δ^{13}C-DOC, subsequent DOC mass-balance

Assumptions and notes:

- Pond water and TOC present similar δ^{13}C-DOC values, so they can be incorporated as a single source into this mixing model (X_1). The second source is DOC in the Holocene aquifer (X_2);
- For aquitard carbon, we employed the δ^{13}C-TOC values from site H and H-200 reported in Eiche et al. (Eiche et al., 2017)* and DOC concentrations from the aquitard pore water extracted at the depths from 16 to 18 m b.g.l.;
- The linear mixing model works when only end members impact the final δ^{13}C-DOC values (i.e. no metabolism is occurring or is occurring at exceptionally low rates).

	δ^{13}C-TOC* + δ^{13}C-DOC Pond **X_1, aquitard+pond**	δ^{13}C-DOC wells 2 and 3 **X_2, Holocene aquifer**	δ^{13}C-DOC wells 6 and 8 **Aquitard/aquifer connections**
δ^{13}C-DOC ‰	-25 (-23/-27)	-30.8 (-30.3/-31.3)	-28.8
Resulting mix	**0.34**	**0.66**	

Test of the δ^{13}C-DOC derived mixing values with DOC concentrations by multiplying the DOC of the sources for the relative mixing ratio:

	DOC aquitard pore water at well 6, 16-18m **X_1, aquitard+pond**	DOC wells 2 and 3 **X_2, Holocene aquifer**	DOC wells 6 and 8 **Aquitard/aquifer connections**
DOC mg C/L	5-8	0.6-2.5	**6.5-7 real**
Mixing ratio from δ^{13}C-DOC	0.34	0.66	
C budget mg C/L	**1.7-2.7**	**0.4-1.65**	**2.1-4.4 model**

This large underestimation of aquitard/pond contribution and the overall DOC budget means that the value of δ^{13}C-DOC = -28.8±1‰ at the aquitard/aquifer connection is not only due to the sources of organic matter. It is likely that TOC in the aquitard is degraded, leading to depletion in the δ^{13}C-DOC signature in the aquitard pore water seeping in the proximity of wells 6 and 8.

Step 3: Mix of N sources from δ^{15}N-NH_4^+, subsequent NH_4^+ mass-balance

Assumptions and notes:

- In this case, pond NH_4^+ presents a different isotopic labelling from that of the aquitard sediments, so we can attempt to estimate the relative proportion of each in terms of organic matter egress into the aquifer;
- In ponds, the NH_4^+ from manure and wastewater (δ^{15}N-NH_4^+ = +5 to +10‰) (Nikolenko et al., 2018) is collected and further enriched in $^{15}NH_4^+$ via evaporation to higher values in the range of δ^{15}N-NH_4^+ = +13±1‰ to +26±1‰;
- For aquitard NH_4^+, we took leachable δ^{15}N-NH_4^+ values measured in a neighbouring village as reported in Norrman et al. (Norrman et al., 2015)** and the NH_4^+ concentrations from aquitard pore water extracted at the depths from 16 to 18 m b.g.l.

	Ponds **X_1, ponds**	Aquitard pore water at well 6, 16-18m and leachable NH_4^+** **X_2, aquitard**	Wells 2 and 3 **X_3, Holocene aquifer**	Wells 6 and 8 **Aquitard/aquifer connections**
δ^{15}N-NH_4^+ ‰	13-26	0-10	5	23
NH_4^+ mg N/L	1-10	16-32	1-16	**50-70 real**
Mixing ratio from $\delta^{18}O/\delta^2H$	0.92		0.08	
Mix from δ^{15}N, within water budget	**0.91-0.92**	**0-0.01**	**0.08**	
NH_4^+ budget mg/L	**1-9**	**0-0.3**	**0.1-1.3**	**1-11 model**

To understand the relative contribution of ponds to NH_4^+ concentrations at the aquitard/aquifer connections, we used a stepwise mixing model, taking into account that ponds and aquitard together contribute 92% of the water recharge at the aquitard/aquifer connections (step 1). Including the δ^{15}N-NH_4^+ values in the calculations, 91% of the NH_4^+ should come from ponds, 1% from the aquitard and 8% from the Holocene aquifer. This mass balance would result in a maximum of 11 mg N/L, a value much lower than the measured 50-70 mg N/L in this well.

This large underestimation of NH_4^+ concentrations means that:

- NH_4^+ must largely come from the pore water in the aquitard, which presents NH_4^+ concentrations closest to those measured in the aquifer. Furthermore, aquitard sediments contain peaty organic matter intercalations with leachable NH_4^+ (Norrman et al., 2015);
- Surficial pond water can indeed percolate through the aquitard, justifying the correctness of stable water isotope signatures and the relative water budgeting calculations, and it receives additional DOC and NH_4^+ from organic matter intercalations;
- The δ^{15}N-NH_4^+ signature from the aquitard sediments can then be enriched in $^{15}NH_4^+$ and attain more positive values as a consequence of other processes occurring in the aquifer, likely NH_4^+ oxidation.

SI.2 Ternary cation diagram

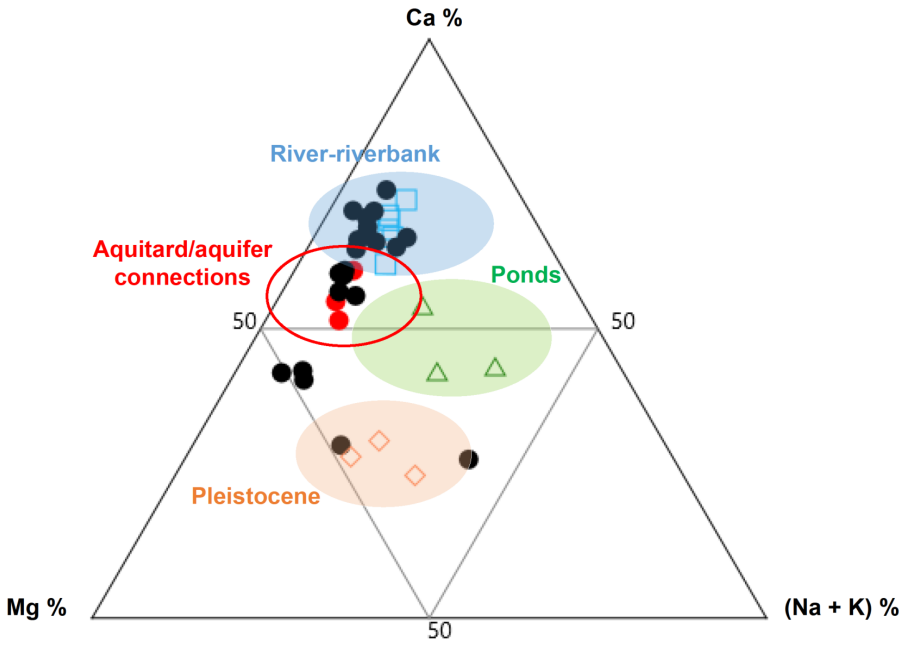

Figure S1: Cation ternary diagram showing the major ion composition of surface and groundwater samples in April 2019. Groundwater samples are indicated with dots, where red dots represent samples collected at the aquitard/aquifer hydraulic connections. The sources of water feeding the aquifer are indicated by colour: river and riverbank samples (squares, blue area), surface ponds (triangles, green area) and Pleistocene wells tapping water most distant from the riverbank (diamonds, orange area). The ternary diagram was generated using PAST software for statistics (Hammer et al., 2001).

The ternary cation diagram (Fig. S1) shows that most of the wells present in Van Phuc receive water from the Red River and infiltrating through the riverbank (blue circle). In addition to this source, the wells with the largest dissolved As and methane concentrations in the upper layers of the Holocene aquifer (red circle) also receive water with a hydrochemical fingerprint similar to that of the surface evaporative water bodies, such as ponds (green circle). This observation provided further evidence for the patchy presence of aquitard/aquifer hydrological connections.

SI.3 Further evaluation of hydrochemical parameters

Well 7a is between the two aquitard/aquifer connections and presents lower total CH_4 concentrations (11 mg/L) compared to the neighbouring wells both upstream and downstream (between 40 and 58 mg/L). At the same time, the δ^{13}C-CH_4 values do not change. Therefore, methane oxidation can be excluded, as it would lead to an increase in δ^{13}C-CH_4 values. The decrease in total CH_4 concentrations could be due to local groundwater dilution with more water from the river and the riverbank, a process that has no net impact on methane isotopy.

A further indication of localised groundwater flow disruption associated with methanogenesis comes from the hydrochemistry of the wells between the aquitard/aquifer connections (Figure 2, well 7 between the arrows indicating aquitard seepage). There, the relative decrease in DOC (from 6.5 to 1.8 mg C/L) is associated with lower δ^{18}O values (from -5.4±0.5 to -6.7±0.5‰) and a cation composition more similar to riverbank water. All these results could indicate the re-intrusion of riverbank water around methanogenic spots, thereby confirming localised flow disruption at the aquitard/aquifer connections.

The largest dissolved Fe values in the Holocene aquifer are not associated with the largest As/methane/DOC concentrations. More Fe is present in wells with more negative δ^{13}C-DOC values associated with fermentative conditions. This seems to support the hypothesis that fermentation can further facilitate Fe(III) reduction, especially in wells where methanogenesis is moderate but not the highest.

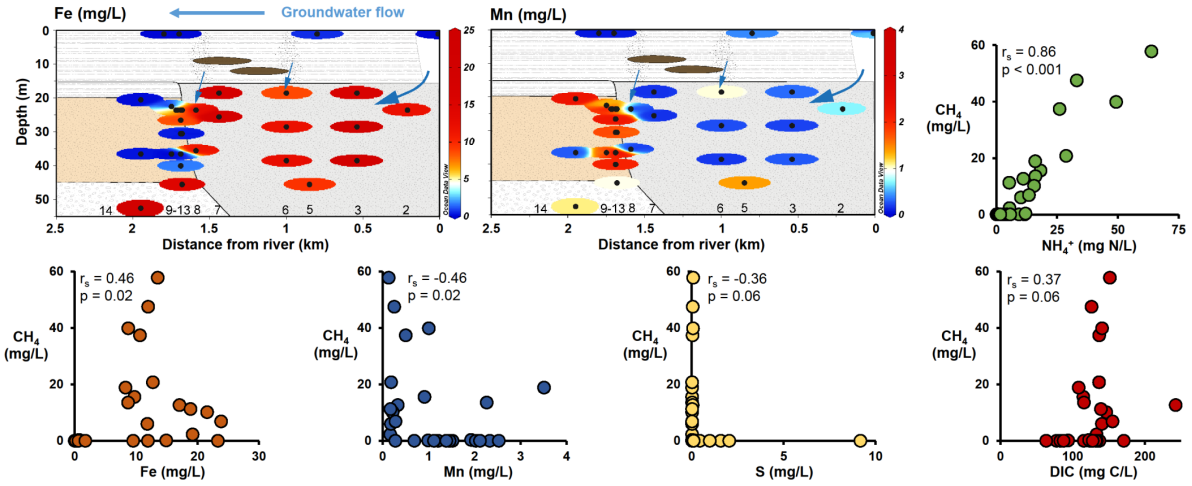

Figure S2: Vertical cross-sections of groundwater parameters along the 2-km transect. Upper left panels: Concentrations of Fe and Mn values in groundwater, surface water and riverbank samples (n_{tot}=38) collected along the studied transect depicted in Figure 1. The black dots indicate the longitudinal positions and depths of the well screens with consecutive well numbers indicated above the x-axes. The colouring is scaled to the maximum value for each parameter and plotted with Ocean Data View (https://odv.awi.de). Blue arrows indicate groundwater flow from the riverbank (flowpath 1) and the aquitard/aquifer hydraulic connections (flowpath 2). The boundaries separating the aquifers and the aquitard are schematically indicated. Surrounding panels: Bivariate plots showing correlations between CH_4 and Fe, Mn, S, DIC and NH_4^+ for the wells along the transect (n=27), with the significance of Spearman's correlation coefficient r_s indicated.

SI.4 Further information about biogeochemical processes based on C isotopes

Prevalence of hydrogenotrophic methanogenesis

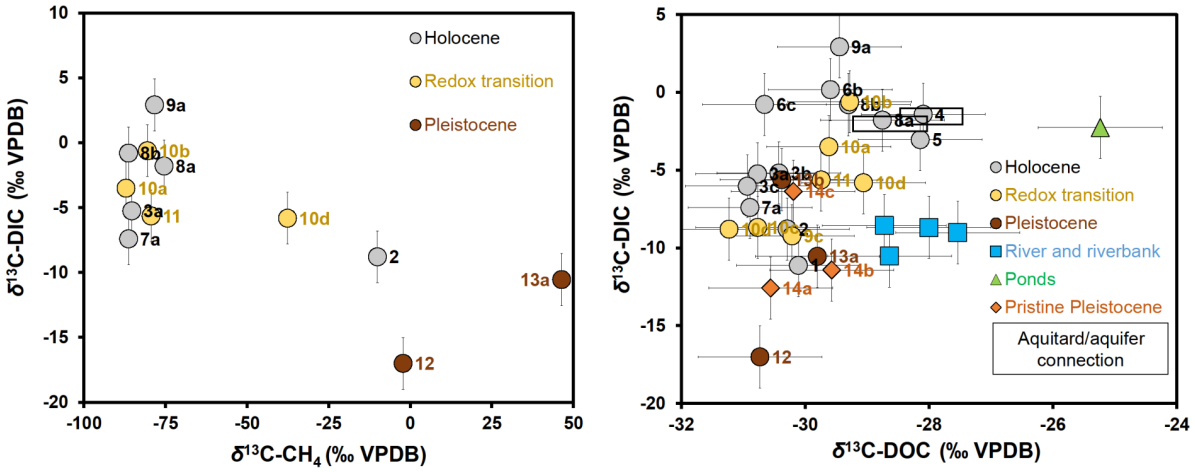

Figure S3: Bivariate plots of: left δ^{13}C-CH_4 and δ^{13}C-DIC; right δ^{13}C-DOC and δ^{13}C-DIC.

In hydrogenotrophic methanogenesis, CO_2 is used as an electron acceptor according to the reaction:

$$CO_2 + 4\ H_2 \rightarrow CH_4 + 2\ H_2O$$

A further methanogenic process, known as acetoclastic methanogenesis, produces both CH_4 and CO_2 from acetic acid:

$$CH_3COOH \rightarrow CH_4 + CO_2$$

While hydrogenotrophic methanogenesis should result in the net production of $^{12}CH_4$ and the accumulation of $^{13}CO_2$, leading to a negative correlation between δ^{13}C-CH_4 and δ^{13}C-DIC, acetoclastic methanogenesis should result in the parallel production of more $^{12}CH_4$ and $^{12}CO_2$, resulting in a positive correlation between δ^{13}C-CH_4 and δ^{13}C-DIC (Whiticar, 1999). The coincidence of high δ^{13}C-DIC values with methanogenic conditions (Fig. S3) suggests that hydrogenotrophic methanogenesis could be dominant.

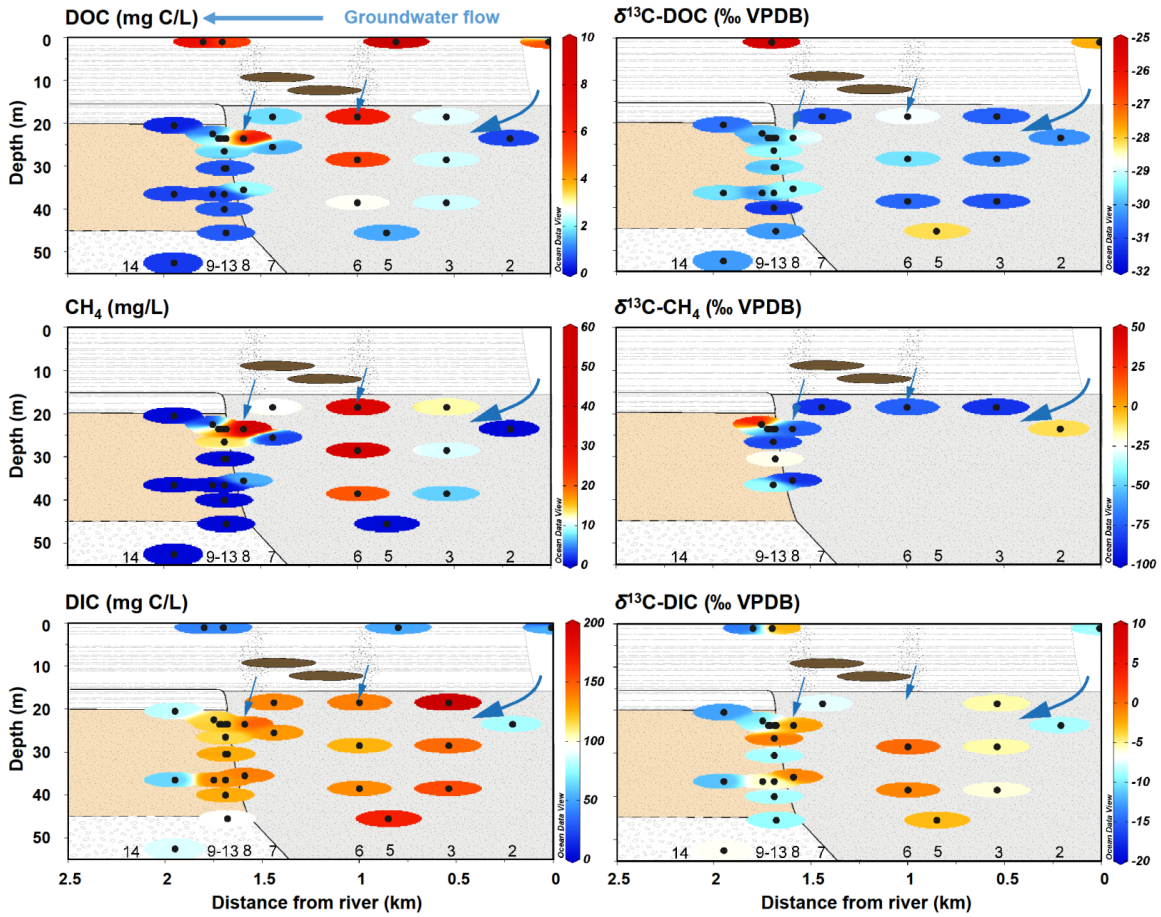

Figure S4: Vertical cross-sections of dissolved carbon species and respective stable carbon isotope values along the 2-km transect. Groundwater, surface water and riverbank samples (n_{tot}=38) collected along the studied transect depicted in Figure 1. The black dots indicate the longitudinal positions and depths of the well screens with consecutive well numbers indicated above the x-axes. The colouring is scaled to the maximum value for each parameter and plotted with Ocean Data View (https://odv.awi.de). Blue arrows indicate groundwater flow from the riverbank (flowpath 1) and the aquitard/aquifer hydraulic connections (flowpath 2). The boundaries separating the aquifers and the aquitard are schematically indicated.

Hydrogenotrophic methanogenesis leads to an average enrichment of -75‰ on DIC (Liu et al., 2009; Conrad et al., 2014). Starting from Van Phuc's DIC, with δ^{13}C-DIC = 0±2‰ to -15±2‰, this would produce a final δ^{13}C-CH_4 = -75±2‰ to -90±2‰. In contrast, acetoclastic methanogenesis would lead to a more moderate depletion of -21‰ on DOC. For Van Phuc's DOC with δ^{13}C-DOC = -25±1‰ to -30±1‰, it would generate a final signature of δ^{13}C-CH_4 = -50±2‰. For methanogenic wells, we

measured $\delta^{13}C\text{-}CH_4$ values from -75±2‰ to -87±2‰, indicating a large contribution of hydrogenotrophic methanogenesis.

The possibility that hydrogenotrophic methanogenesis biases $\delta^{18}O\text{-}H_2O$ and $\delta^{2}H\text{-}H_2O$ towards more negative values is highly unlikely. First, for the case of 60 mg CH_4/L generation, this is equal to 4 mmol/L of methane and 8 mmol/L of water produced by hydrogenotrophic methanogenesis. This amount of water generated is minor compared to the 55.6 moles of water per litre on which a stable water isotope analysis is based. This approximate calculation also helps to clarify the fact that $\delta^{18}O\text{-}H_2O$ and $\delta^{2}H\text{-}H_2O$ values refer to the source of water and that the impact of biological processes is minimal. In addition, we did observe enrichment in $\delta^{18}O\text{-}H_2O$ and $\delta^{2}H\text{-}H_2O$ rather than a depletion in the methanogenic wells at the aquitard/aquifer connection.

Fermentative processes contribute to the decrease in $\delta^{13}C$-DOC in groundwater samples all across the aquifers (Conrad et al., 2014). Unfortunately, the large variability of the $\delta^{13}C$-DIC values caused by methanogenic and methanotrophic processes as well as the co-occurrence of other organic matter oxidising processes complicates any attempts to delve further into the relative contribution of different fermentative processes by comparing the $\delta^{13}C$-DIC and $\delta^{13}C$-DOC values.

Empirical methane fractionation factors

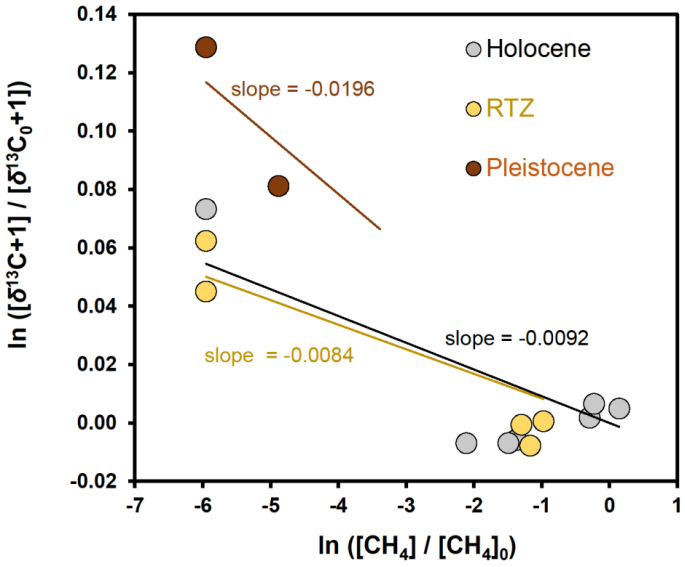

Figure S5: Evaluation of site-specific methane transformation along the studied transect based on normalised methane concentrations.

We adopted a calculation approach as reported in Aeppli et al. (Aeppli et al., 2009; Aeppli et al., 2010). The goal was to test whether in the different portions of the aquifers, different processes involving methane are occurring, hence leading to different methane fractionation rates. We assumed that the system is closed, a background concentration of methane of 50 mg/L, coinciding with its saturation limits, and a $\delta^{13}C_0$ value of -80‰. The concentrations and isotopic signatures of each sample are subsequently scaled to these values. The slopes of the so-obtained linear interpolations coincide with ε/1000, imposing passage through zero. Despite the limited number of samples, enrichment factors were calculated for methane transformation in the Holocene aquifer and the RTZ. They differed clearly from the Pleistocene aquifer, i.e. $\varepsilon_{Holocene}$ = 9.2‰, ε_{RTZ} = 8.4‰, $\varepsilon_{Pleistocene}$ = 19.6‰. These results could indicate that similar reactions lead to methane production and consumption in the Holocene aquifer and at the RTZ, while different and/or additional methane transformation mechanisms occur in the Pleistocene aquifer.

SI.5 N isotopes provide additional insights into the sources of dissolved organic matter

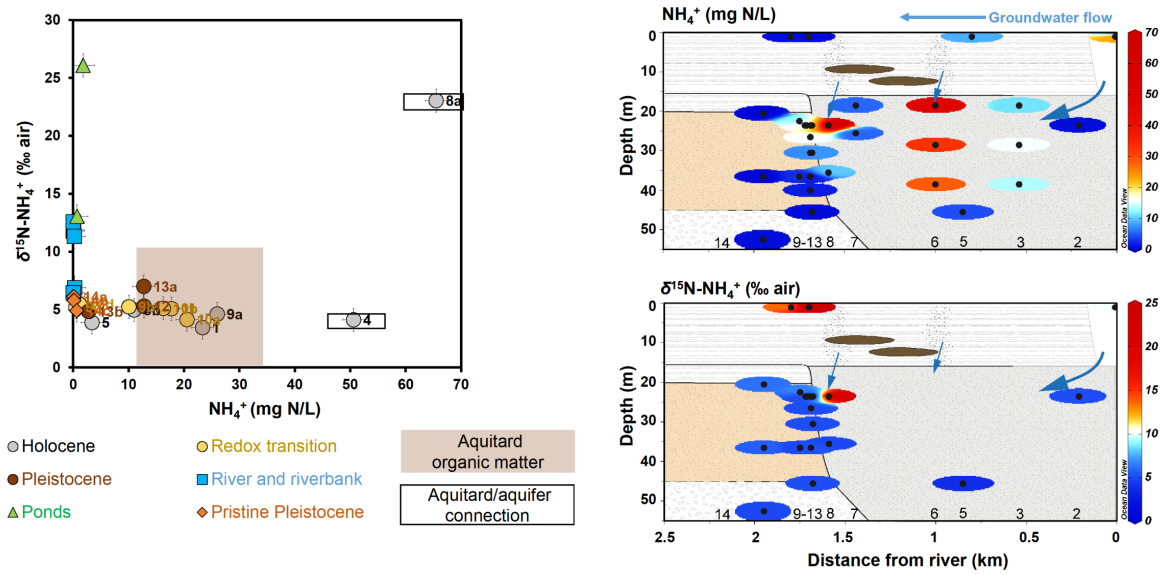

Figure S6: Plots of δ^{15}N-NH_4^+ values and total NH_4^+ concentrations. Left: Bivariate plot for wells in the Holocene aquifer (grey circles), at the redox transition (yellow circles) and in the Pleistocene aquifer (brown circles). The brown box represents the values associated with organic matter intercalations within the aquitard, with δ^{15}N-NH_4^+ values from Norrman et al. (Norrman et al., 2015), and NH_4^+ concentrations from aquitard pore water extracted at the depths from 16 to 18 m b.g.l. (supplementary material, Section SI.1). Right: Vertical cross-sections along groundwater flow direction of δ^{15}N-NH_4^+ values. Wells are indicated by a number, representing the progressive distance from the river, and a letter for increasing depth in cases of multiple wells (Table S1 for the original data). Data collected in June 2018, Van Phuc village, Vietnam.

The δ^{15}N-NH_4^+ values in the groundwater vary between +3±1‰ and +7±1‰ (Fig. S6), a range that is compatible with the values of leachable NH_4^+ measured in the sediments of a neighbouring village (0 to +10±1‰ (Norrman et al., 2015). Similar to TOC, the aquifer sediments contain almost no N (average <0.03 wt.%) (Eiche et al., 2017). Therefore, the NH_4^+ in the groundwater samples is most likely derived from the degradation of organic matter intercalations in the aquitard and in riverbank sediments.

One well below an aquitard/aquifer connection presents a $\delta^{15}N\text{-}NH_4^+$ value of +23±1‰ (Fig. S6, well 8a). This value is in the range of NH_4^+ in ponds in the village, where NH_4^+ from manure and fertilisers is enriched by evaporation and would suggest the localised direct seepage of pond-derived NH_4^+ into the aquifer. As such, $\delta^{15}N\text{-}NH_4^+$ signatures would allow for disentangling the pond (+13/+26‰) and aquitard pore water (0/+10‰) NH_4^+ contribution to the aquifer at the aquitard/aquifer connections. Still, the N mass balance (see the supplementary material section SI.1 for details) indicates that the majority of NH_4^+ in the wells below the aquitard/aquifer connection (50-70 mg N/L) likely originates from the leached aquitard pore water (where NH_4^+ increases from 16 to 30 mg N/L between 16 and 18 m depth) and not from ponds (1-10 mg N/L).

Therefore, other processes should cause the observed isotopic enrichment of aquitard pore water NH_4^+ below the aquitard/aquifer connection. One possibility is an in-aquifer degassing of NH_3 (Norrman et al., 2015). The pH value of 7.4 at this well implies that NH_4^+, and not NH_3, is the dominant species (98% NH_4^+ and 2% NH_3 in equilibrium under standard conditions). Furthermore, NH_4^+ and $\delta^{15}N\text{-}NH_4^+$ are anti-correlated (i.e. the opposite of what is expected for degassing), and hence large NH_3 degassing seems unlikely. The second process is NH_4^+ oxidation. Putative NH_4^+-oxidizing bacteria are present in the groundwater at the Van Phuc site (Glodowska et al., 2021). While looking for metabolites of NH_4^+ oxidation, we indeed detected trace amounts of both NO_2^- and N_2O in the groundwater samples. Such below-quantification abundance does not exclude the occurrence of N-cycling with rapid turnover rates of metabolites and reactions such as Feammox, where NH_4^+ oxidation is coupled with Fe(III) reduction and As mobilisation (Weng et al., 2017).

References

Aeppli, C., Berg, M., Cirpka, O.A., Holliger, C., Schwarzenbach, R.P., Hofstetter, T.B., 2009. Influence of Mass-Transfer Limitations on Carbon Isotope Fractionation during Microbial Dechlorination of Trichloroethene. Environmental Science & Technology 43, 8813-8820.

Aeppli, C., Hofstetter, T.B., Amaral, H.I.F., Kipfer, R., Schwarzenbach, R.P., Berg, M., 2010. Quantifying In Situ Transformation Rates of Chlorinated Ethenes by Combining Compound-Specific Stable Isotope Analysis, Groundwater Dating, And Carbon Isotope Mass Balances. Environmental Science & Technology 44, 3705-3711.

Conrad, R., Claus, P., Chidthaisong, A., Lu, Y., Fernandez Scavino, A., Liu, Y., Angel, R., Galand, P.E., Casper, P., Guerin, F., Enrich-Prast, A., 2014. Stable carbon isotope biogeochemistry of propionate and acetate in methanogenic soils and lake sediments. Organic Geochemistry 73, 1-7.

Eiche, E., Berg, M., Hönig, S.-M., Neumann, T., Lan, V.M., Pham, T.K.T., Pham, H.V., 2017. Origin and availability of organic matter leading to arsenic mobilisation in aquifers of the Red River Delta, Vietnam. Applied Geochemistry 77, 184-193.

Glodowska, M., Stopelli, E., Straub, D., Vu Thi, D., Trang, P.T.K., Viet, P.H., AdvectAs team, m., Berg, M., Kappler, A., Kleindienst, S., 2021. Arsenic behavior in groundwater in Hanoi (Vietnam) influenced by a complex biogeochemical network of iron, methane, and sulfur cycling. Journal of Hazardous Materials 407, 124398.

Hammer, Ø., Harper, D.A.T., Ryan, P.D., 2001. PAST: paleontological statistics software package for education and data analysis. Palaeontologia Electronica 4, 1-9.

IAEA, 2001. Environmental isotopes in the hydrological cycle. Principles and applications. International Atomic Energy Agency, Vienna. http://www-naweb.iaea.org/napc/ih/IHS_resources_publication_hydroCycle_en.html

Liu, T.-K., Chen, K.-Y., Yang, T.F., Chen, Y.-G., Chen, W.-F., Kang, S.-C., Lee, C.-P., 2009. Origin of methane in high-arsenic groundwater of Taiwan – Evidence from stable isotope analyses and radiocarbon dating. Journal of Asian Earth Sciences 36, 364-370.

Nikolenko, O., Jurado, A., Borges, A.V., Knöller, K., Brouyère, S., 2018. Isotopic composition of nitrogen species in groundwater under agricultural areas: A review. Science of The Total Environment 621, 1415-1432.

Norrman, J., Sparrenbom, C.J., Berg, M., Dang, D.N., Jacks, G., Harms-Ringdahl, P., Pham, Q.N., Rosqvist, H., 2015. Tracing sources of ammonium in reducing groundwater in a well field in Hanoi (Vietnam) by means of stable nitrogen isotope (δ15N) values. Applied Geochemistry 61, 248-258.

Stopelli, E., Duyen, V.T., Mai, T.T., Trang, P.T.K., Viet, P.H., Lightfoot, A., Kipfer, R., Schneider, M., Eiche, E., Kontny, A., Neumann, T., Glodowska, M., Patzner, M., Kappler, A., Kleindienst, S., Rathi, B., Cirpka, O., Bostick, B., Prommer, H., Winkel, L.H.E., Berg, M., 2020. Spatial and temporal evolution of groundwater arsenic contamination in the Red River delta, Vietnam: Interplay of mobilisation and retardation processes. Science of The Total Environment 717, 137143.

Weng, T.-N., Liu, C.-W., Kao, Y.-H., Hsiao, S.S.-Y., 2017. Isotopic evidence of nitrogen sources and nitrogen transformation in arsenic-contaminated groundwater. Science of The Total Environment 578, 167-185.

Whiticar, M.J., 1999. Carbon and hydrogen isotope systematics of bacterial formation and oxidation of methane. Chemical Geology 161, 291-314.